Eur. J. Mech. B - Fluids 19 (2000) 559–574

S0997-7546(00)00101-1/FLA

Global modes and superdirective acoustic radiation in low-speed axisymmetric jets

Alison J. Cooper *, David G. Crighton

Department of Applied Mathematics and Theoretical Physics,
University of Cambridge, Silver Street, Cambridge, CB3 9EW, UK

(Received 2 April 1999; revised 20 August 1999; accepted 16 September 1999)

Abstract – Global linear stability theory is used to study the resonances in a slowly diverging axisymmetric jet. The absolute frequency ω_0 is calculated as a function of slow axial position X, and analytic continuation into the complex X-plane allows a saddle point in ω_0 to be identified. A key element in the analysis is the approximation of $\omega_0(X)$ by rational functions which identifies a well-defined saddle point and leading-order global frequency. A preferred-mode Strouhal number, $S_D = 0.44$, is calculated which compares well with existing experimental values. The global frequency has negative imaginary part and the jet is interpreted as being marginally globally stable, so that forcing in the vicinity of the resonance frequency produces a large response above background, rather like that of a slightly damped linear oscillator. The axial shape of the global-mode amplitude is Gaussian and yields a superdirective acoustic field. © 2000 Éditions scientifiques et médicales Elsevier SAS

global mode / axisymmetric jet / resonance / superdirectivity / Remes algorithm

1. Introduction

In practical cases jet noise fields are generated by jet flows subject to external forcing, usually through fluctuations upstream of the nozzle exit. Such forcing, if suitably coherent, stimulates large-scale coherent structures of the jet-column mode kind. These structures have often been modelled as axisymmetric (or low-order azimuthal) spatial instability waves, of each frequency present in the forcing. In this view the jet is simply an amplifier of external fluctuations. Various calculations have been made to determine the curve of amplification as a function of fluctuation frequency and other parameters (Crow and Champagne [1]; Michalke [2]; Crighton and Gaster [3]), although these calculations, and the prediction of the associated acoustic fields, have met with limited success. An alternative view regards the jet as a resonator, whose lowest modes are slightly damped and have resonance frequencies with small imaginary parts. These global mode frequencies are preferentially filtered out of a general nozzle exit forcing. The axial shape function of the lowest order global mode can be expected to be Gaussian, as shown by the general theory of global modes developed by Monkewitz, Huerre and Chomaz [4] and other collaborators. A Gaussian shape function, together with appropriate parameters, is precisely what is needed to yield a superdirective (beaming) acoustic field, according to the theory of Crighton and Huerre [5], and in agreement with the measurements of Laufer and Yen [6] on very low speed jets.

Under certain flow conditions, many spatially developing shear flows exhibit self-sustained oscillations with the result that near-field large-scale dynamics become effectively tuned at a specific frequency. The spatio-temporal distribution of fluctuations then defines the global mode associated with the flow. Typical examples of flows which exhibit self-sustained oscillations are wakes and hot jets. Huerre and Monkewitz [7] and Chomaz,

* Correspondence and reprints; e-mail: A.J.Cooper@damtp.cam.ac.uk

Huerre and Redekopp [8] have shown that a region of local absolute instability is necessary for the existence of globally unstable flows. Here we examine the case of an axisymmetric cold jet where local instability analysis shows that, although the flow does not produce a pocket of absolute instability, it can be described as being marginally globally stable. Analysis is restricted to axisymmetric modes, which are simple to excite in experimental investigations and are more unstable in the potential core region of the jet than higher-order azimuthal modes.

In marginally globally stable flows, the response to forcing becomes similar to that of a slightly damped linear oscillator, in that forcing close to the resonance frequency gives rise to a large response above background. The existence of a resonance, or preferred, frequency agrees with the behaviour observed in experimental investigations where a preferred jet-column mode is evident. The idea of using a global mode framework to analyze the jet-column mode was originally developed by Huerre and Monkewitz [7]. They adapted a Ginzburg–Landau model and showed that the response to forcing was exactly that of a slightly damped linear oscillator close to resonance. The theory of global modes thus predicts a well-defined resonance frequency, whereas there is no definite frequency selection using locally parallel stability theory.

The method of determining the global modes associated with a spatially developing flow is applied to the specific example of an axisymmetric 'near-top-hat' jet flow which models that studied experimentally by Crow and Champagne [1] and Laufer and Yen [6] amongst many others. This jet flow (actually the mean flow of a turbulent jet) is assumed to be weakly non-parallel so that global modes can be studied using the WKBJ-type of analysis developed by Monkewitz et al. [4]. The preferred mode Strouhal number associated with this flow can be determined using the local instability properties on the real axial (X) axis. Absolute frequencies and wavenumbers are calculated in accordance with the criterion of Briggs [9] and Bers [10,11]. This imposes conditions on the origins of the spatial branches that give rise to pinching in the complex frequency plane, and allows the absolute frequency to be correctly identified. Once values along the real X-axis have been determined, analytic continuation is used to immerse the problem in the complex X-plane. This allows the location of saddle points in the absolute frequency to be determined which, in turn, gives the leading-order estimate of the global frequency.

Section 2 describes the governing equations and local stability analysis and section 3 outlines the global frequency calculation leading to expressions for the global-mode frequency. Section 4 introduces the analytical form used for the jet mean flow. In section 5 the numerical procedure used to solve the governing stability equation is described, followed by the method of analytic continuation used in the determination of the saddle-point location. Numerical results are then presented for the global-mode frequency and other parameters, and comparisons are made with experimentally determined quantities.

2. Governing equations and stability analysis

The flow problem for the slowly diverging axisymmetric jet is formulated in terms of cylindrical coordinates (x^*, r^*, θ) (where superscript '*' is used throughout to denote a dimensional quantity). The total streamfunction consists of a time-independent mean flow $\bar{\psi}^*(x^*, r^*)$ and an unsteady perturbation of axisymmetric disturbances $\widehat{\psi}^*(x^*, r^*, t^*)$. In this case the jet mean flow has an analytical form fitted to experimental measurements. The total streamfunction is

$$\psi^*(x^*, r^*, t^*) = \bar{\psi}^*(x^*, r^*) + \widehat{\psi}^*(x^*, r^*, t^*),$$

and $u_x^* = (1/r^*)\partial\psi^*/\partial r^*$ and $u_r^* = -(1/r^*)\partial\psi^*/\partial x^*$.

In jet-flow problems there exist two length scales, the shear-layer thickness δ^*, and the jet exit radius $D^*/2$. In order to non-dimensionalize the problem all lengths are scaled with respect to the radius $D^*/2$ and velocities with respect to the mean centre-line velocity U_0^*, so that the dimensionless variables are

$$r = \frac{2r^*}{D^*}, \qquad x = \frac{2x^*}{D^*}, \qquad u = \frac{2u^*}{U_0^*}, \qquad t = \frac{U_0^* t^*}{D^*}.$$

Substitution of the streamfunction into the incompressible Euler equations and linearizing with respect to the perturbation leads to the following equation for the perturbation $\widehat{\psi}$:

$$\begin{aligned}\left[\frac{\partial}{\partial t} + U\frac{\partial}{\partial x}\right]\left[\frac{\partial^2\widehat{\psi}}{\partial x^2} + \left(\frac{\partial^2\widehat{\psi}}{\partial r^2} - \frac{1}{r}\frac{\partial\widehat{\psi}}{\partial r}\right)\right] - \left(\frac{\partial^2 U}{\partial r^2} - \frac{1}{r}\frac{\partial U}{\partial r}\right)\frac{\partial\widehat{\psi}}{\partial x}\\ = \left[-V\frac{\partial}{\partial r} + \frac{2V}{r}\right]\left[\frac{\partial^2\widehat{\psi}}{\partial x^2} + \left(\frac{\partial^2\widehat{\psi}}{\partial r^2} - \frac{1}{r}\frac{\partial\widehat{\psi}}{\partial r}\right)\right] + \left(\frac{\partial\widehat{\psi}}{\partial r}\frac{\partial}{\partial x} - \frac{\partial\widehat{\psi}}{\partial x}\frac{\partial}{\partial r} + \frac{1}{r}\frac{\partial\widehat{\psi}}{\partial x}\right)\frac{\partial V}{\partial x} - \frac{\partial\widehat{\psi}}{\partial r}\frac{\partial^2 U}{\partial x\,\partial r}, \quad (1)\end{aligned}$$

where the non-dimensional mean velocity field is denoted by $[U(x,r), V(x,r)]$. Terms appearing on the right-hand side arise from the non-parallel form of the mean flow.

The mean flow is assumed to be weakly non-parallel, so that it depends in the streamwise direction on the 'slow' coordinate $X = \varepsilon x$, where $\varepsilon \ll 1$ and is a measure of the divergence rate of the jet in relation to a disturbance of $O(D^*)$, so that $\varepsilon \sim \mathrm{d}(\delta^*/D^*)/\mathrm{d}(x^*/D^*)$. It should be noted that this weakly non-parallel flow assumption restricts any viscous effects to $O(\varepsilon)$ and for the mean flow under investigation the rescaling results in $U = O(1)$ and $V = O(\varepsilon)$. The aim now is to determine the causal Green's function, $G(x,r,t)$, of (1) with the introduction of a source term in (1).

In order to proceed the Fourier transform of (1) is taken in time, with

$$\hat{G}(x,r,\omega) = \int_{-\infty}^{\infty} G(x,r,t)\exp(i\omega t)\,\mathrm{d}t, \quad (2)$$

and the standard form of the WKBJ approximation (see Bender and Orszag [12]; Monkewitz et al. [4]) used for the Green's function. This gives

$$\hat{G}^{\pm} \sim \left[\hat{G}_0^{\pm}(X,r) + \varepsilon\hat{G}_1^{\pm}(X,r) + O(\varepsilon^2)\right]\exp\left[\frac{i}{\varepsilon}\int_{X_s}^{X} k^{\pm}(X';\omega)\,\mathrm{d}X'\right], \quad (3)$$

where '+' and '−' correspond to solutions downstream and upstream of the source respectively, and $k^{\pm}$ denote local wavenumbers originating in the upper and lower halves of the k-plane respectively. X_s is the axial location of the source on the jet centreline, and only axisymmetric modes are considered.

Successive terms in the expansion of $\hat{G}^{\pm}$ are determined using the method of multiple scales. By using the chain rule

$$\frac{\partial}{\partial x} \to \frac{\partial}{\partial x} + \varepsilon\frac{\partial}{\partial X},$$

and introducing the expansion for $\hat{G}^{\pm}$ in (1), a series of locally parallel problems are generated at each order in ε.

At $O(\varepsilon^0)$, $\hat{G}_0^{\pm}$ must satisfy the homogeneous Rayleigh equation:

$$O(\varepsilon^0):\ \mathcal{L}\{\phi_0^{\pm}; k^{\pm}, \omega, X\} = 0, \quad \phi_0^{\pm}(r\to 0)\ \text{finite},\ \phi_0^{\pm}(r\to\infty) = 0, \quad (4)$$

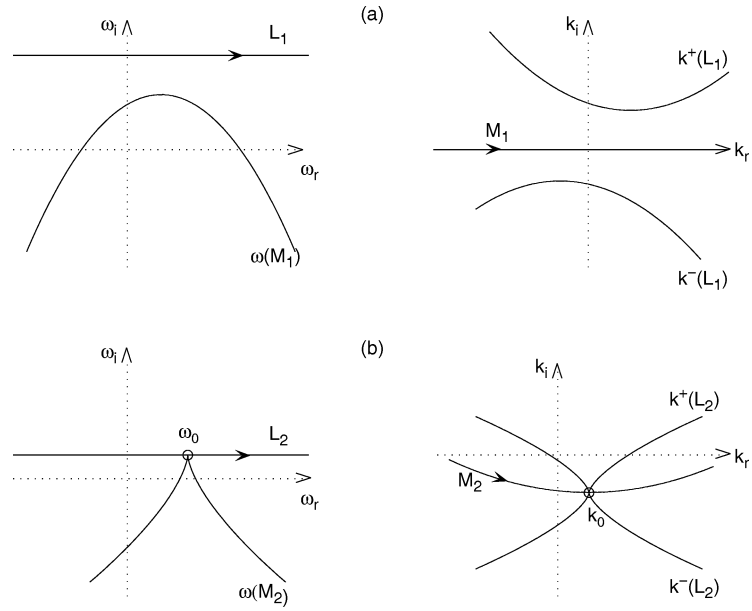

Figure 1. Sketches of a temporal branch of the dispersion relation given by the M-contour and spatial branches given by the L-contour when X is fixed at some real value. The branches deform from their positions in (a) until pinching at (ω_0, k_0) occurs as shown in (b).

where

$$\mathcal{L}\{\cdot\} \equiv \left[kU(X,r) - \omega\right]\left[\left(\frac{\partial^2}{\partial r^2} - \frac{1}{r}\frac{\partial}{\partial r}\right) - k^2\right]\{\cdot\} - k\left[\left(\frac{\partial^2}{\partial r^2} - \frac{1}{r}\frac{\partial}{\partial r}\right)U(X,r)\right]\{\cdot\}, \tag{5}$$

and

$$\hat{G}_0^{\pm}(X,r) = A_0^{\pm}(X)\phi_0^{\pm}(r;X). \tag{6}$$

The amplitude $A_0^{\pm}$ is determined at the next order in ε, where a secularity condition must be satisfied.

3. Global-mode structure

We are particularly interested in the long-time behaviour of the Green's function, G, and the global-mode structure associated with this. The main steps are summarized here but the reader is referred to the general theory of Monkewitz et al. [4] for a more detailed explanation.

The long-time behaviour of G is determined by the uppermost singularity of $\hat{G}$ in the ω-plane. In a strictly parallel flow problem the associated pole is the absolute frequency $\omega_0 \equiv \omega(k_0)$. This is defined as the frequency at which the two spatial branches k^+ and k^- coalesce in the complex k-plane. At this point $k^{\pm} = k_0$ and $\omega_0 = \omega(k_0)$. The spatial branches, however, must satisfy the Briggs–Bers criterion (Briggs [9]; Bers [10,11]). This states that in order to satisfy causality, the two spatial branches must originate in opposite halves of the complex k-plane when the imaginary part of ω (ω_i) is sufficiently large to exceed any possible temporal growth rates. As the ω-contour is lowered the spatial branches move and in order for the integration path to pass between them it must be deformed off the real k-axis. Lowering of the ω-contour continues until the integration path becomes pinched between the k^+ and k^- branches at the saddle point k_0, where $\partial\omega/\partial k = 0$ (see *figure 1*). If the flow is weakly non-parallel, then there exists a value of ω_0 for each value of X on the real axis and in an analogous way $\hat{G}(X;\omega)$ becomes singular at some value X^t in the complex X-plane from which

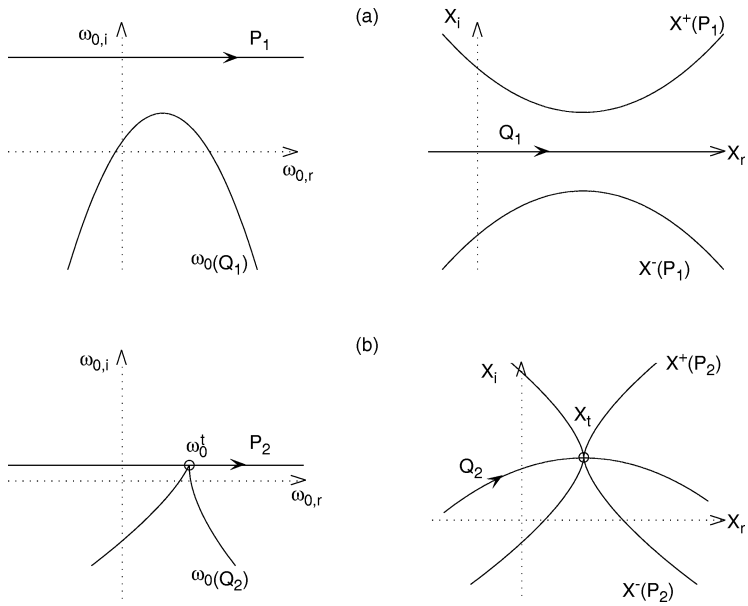

Figure 2. Evolution of branches in ω_0 and X-planes as the ω_0-integration contour is lowered from P_1 to P_2. $Q_{1,2}$ are the corresponding X-integration contours.

the X-integration contour cannot be moved (see *figure 2*). The long-time behaviour of $\hat{G}$ is therefore governed by the saddle point, or second-order turning point, X^t, where the following conditions must be satisfied:

$$\frac{\partial\omega}{\partial X}(k_0^t; X^t) = 0, \qquad \frac{\partial\omega}{\partial k}(k_0^t; X^t) = 0, \qquad \omega_0^t \equiv \omega(k_0^t; X^t). \tag{7}$$

The importance of considering the complex X-plane has been highlighted in the field of quantum mechanics where work on bound states in potential-well problems (Pokrovskii and Khalatnikov [13]; Hille [14]; Bender and Orszag [12]) corresponds closely with work on global modes in fluid stability problems. Stokes had also shown that it is important to study the physical problem in the complex X-plane, suggesting that branch switching at some complex value of X may significantly affect the behaviour at real X.

Once X^t has been identified a rescaling is carried out in the turning point region. Assuming a doubly infinite flow domain, the long-time response of G is dominated by the global frequency ω_G which has leading order contribution ω_0^t and a small correction term $\varepsilon\omega_2$ such that

$$\omega_G = \omega_0^t + \varepsilon\omega_2. \tag{8}$$

In the turning-point region, the disturbance streamfunction is expanded as

$$\widehat{\psi}' = \left[\Phi_0 + \varepsilon^{1/2}\Phi_1 + \varepsilon\Phi_2 + \mathrm{O}(\varepsilon^{3/2})\right](\bar{X}, r)\exp\left[\frac{i}{\varepsilon}k_0^t(X - X^t) - i\omega_G t\right], \tag{9}$$

where $\bar{X} \equiv \varepsilon^{-1/2}(X - X^t)$ and $k_0^t \equiv k_0(X^t)$. The leading-order solution is

$$\Phi_0(\bar{X}, r) = \bar{A}_0(\bar{X})\phi_0^t(r), \tag{10}$$

where ϕ_0^t is the solution to the $O(\varepsilon^0)$ (Rayleigh) problem. (Superscript 't' from hereon refers to evaluation at $X = X^t$.) At higher order, a solvability condition generates a linearized Ginzburg–Landau equation with variable coefficients for the amplitude $\bar{A}_0$. This is solved through the introduction of a new variable

$$\xi \equiv \left(\frac{4\omega_{0XX}^t}{\omega_{kk}^t}\right)^{1/4} \bar{X}, \tag{11}$$

where $\omega_{0XX} \equiv \partial^2\omega_0/\partial X^2$ and $\omega_{kk} \equiv \partial^2\omega/\partial k^2$. If the amplitude function is set to

$$\bar{A}_0(\bar{X}) = \exp\left[\frac{1}{2} i k_{0X}^t \bar{X}^2\right] \alpha(\xi), \tag{12}$$

where $k_{0X} \equiv \partial k_0/\partial X$, then this leads to the standard Hermite equation for $\alpha(\xi)$ (see Monkewitz et al. [4] for details), and in order that turning point region solutions match the WKBJ solutions both upstream and downstream of X^t, the frequency correction ω_2 (and hence ω_G) is restricted to a set of discrete values such that

$$\omega_{Gn} = \omega_0^t + \varepsilon\omega_{2n} = \omega_0^t + \varepsilon\left[\delta\omega^t - \frac{1}{2} i \omega_{kk}^t k_{0X}^t + \left(n + \frac{1}{2}\right)\left(\omega_{kk}^t \omega_{0XX}^t\right)^{1/2}\right], \tag{13}$$

where n is an integer and $\delta\omega^t$ arises from non-parallel and viscous effects (a truly non-local effect). The corresponding eigenfunctions are

$$\alpha_n(\xi) = \exp\left[-\frac{1}{4}\xi^2\right] \mathrm{He}_n(\xi), \tag{14}$$

where $\mathrm{He}_n(\xi)$ are Hermite polynomials. Thus the lowest-order ($n = 0$) global eigenfunction has the Gaussian form

$$\bar{A}_0(\bar{X}) = \exp\left[-\frac{1}{2}\left\{\left(\frac{\omega_{0XX}^t}{\omega_{kk}^t}\right)^{1/2} - i k_{0X}^t\right\}\bar{X}^2\right]. \tag{15}$$

This analysis will be applied to a specific jet profile in the next section. The above frequency selection criterion can be used to determine the preferred-mode Strouhal number by locating the saddle-point X^t in the complex X-plane. The calculated Strouhal number, based on jet exit diameter, is obtained from the leading-order contribution to the global frequency as follows

$$S_D = \frac{f^* D^*}{U_0^*} = \frac{\omega^* D^*}{2\pi U_0^*} \sim \frac{\omega_{G0,r}}{2\pi} \sim \frac{\omega_{0,r}^t}{2\pi},$$

where subscript 'r' refers to the real part. The following sections introduce the specific jet profile used in the analysis and describe the numerical procedures needed to carry out the preceding analysis.

4. Mean jet profile

The jet profile used for this investigation is the 'near-top-hat' profile introduced by Crighton and Gaster [3] which is dependent on x^*. The diverging jet profile shows good agreement with experimental data up to $x^* \approx 4D^*$ (see Strange and Crighton [15]), and can in this sense be taken as satisfying the mean turbulence equations. Strange and Crighton [15] give the arguments by which stability analyses can be applied in this way to the mean profile of a turbulent jet.

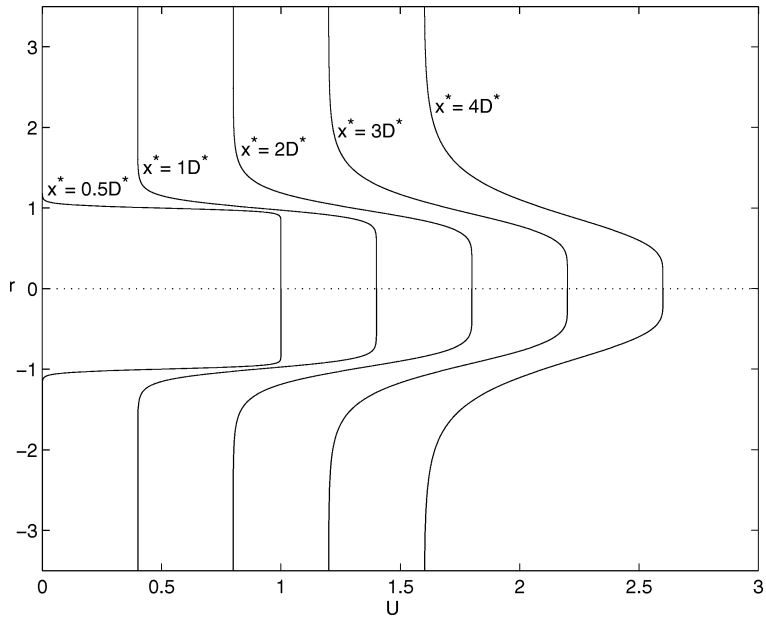

Figure 3. Radial distributions of the mean jet profile at various streamwise positions suggesting the spatial structure of the jet.

The analytical form of this profile is

$$U^*(x^*, r^*) = \frac{U_0^*}{2}\left[1 + \tanh\left\{\frac{D^*}{2(\delta_0^* + \delta' x^*)}\left(\frac{D^*}{2r^*} - \frac{2r^*}{D^*}\right)\right\}\right], \tag{16}$$

where δ' is the shear layer divergence rate and δ_0^* is the initial shear-layer thickness. Using the non-dimensionalization scheme introduced earlier, and taking $\varepsilon = \delta'/2$ for the slow scale, the non-dimensional form of the profile is

$$U(X, r) = 1 + \tanh\left[\frac{1}{2(d + X)}\left\{\frac{1}{r} - r\right\}\right], \tag{17}$$

where $d = \delta_0^*/D^*$. The velocity profile at selected streamwise positions is shown in *figure 3*. Near the nozzle the profile is indeed close to a top-hat, with narrow shear layers. Not much remains of the uniform 'potential core' beyond about $x^* = 5D^*$ or so.

5. Mathematical methods

5.1. Numerical solution of the Rayleigh equation

The Rayleigh equation appearing in (5) was solved numerically using a fourth-order Runge–Kutta integration scheme to compute the eigenvalues. For the velocity profile under consideration $\partial^2 U/\partial r^2, \partial U/\partial r \to 0$ as $r \to 0, \infty$ which reduces the Rayleigh equation, in those limits, to the modified Bessel equation

$$\frac{\mathrm{d}^2\phi_0}{\mathrm{d}r^2} + \frac{1}{r}\frac{\mathrm{d}\phi_0}{\mathrm{d}r} - k^2\phi_0 = 0. \tag{18}$$

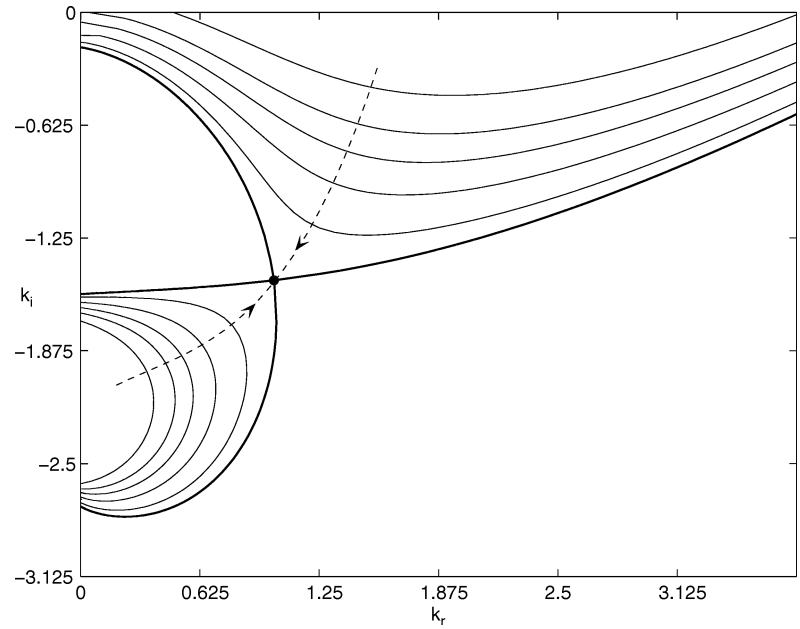

Figure 4. Evolution of the $k^{\pm}$-branches as ω_i is decreased to $\omega_{0,i}$ (thick lines). Arrows indicate the direction of movement of the k-branches and the dashed line indicates the path of $\omega_{0,r}$. The circle denotes the value of k_0. The curves shown are for $\omega_i = 0.015,\ 0.0,\ -0.01,\ -0.02,\ -0.03,\ -0.03588$ (thick line).

Physical boundary conditions require that ϕ_0/r and ϕ_0'/r are finite at $r = 0$ and tend to zero as $r \to \infty$. This requirement then defines appropriate boundary conditions for the numerical problem. Using the general solution to the Bessel equation we find that

$$\phi_0 \sim Ar I_1(kr) \sim Akr^2 \quad \text{as } r \to 0, \tag{19}$$

$$\phi_0 \sim Br K_1(kr) \sim Be^{-kr}\left(\frac{r}{k}\right)^{1/2} \quad \text{as } r \to \infty, \tag{20}$$

where I and K denote modified Bessel functions of the first and second kinds, and A, B are arbitrary constants.

The eigenvalues are found by integrating the Rayleigh equation in both forward and backward directions with (19) and (20) as starting values. An iteration scheme is used to obtain smooth matching of the solutions at some intermediate value r_m. This fixes the constant B, with A left as a free normalization constant.

5.2. Absolute frequency calculation

The absolute frequency ω_0 is defined as the frequency at which the two branches k^+ and k^- coalesce in the complex k-plane; at this point $k^{\pm} = k_0$, and $\omega_0 = \omega(k_0)$. These branches, however, must satisfy the criterion of Briggs and Bers (Briggs [9]; Bers [10,11]), which imposes conditions on the origins of the spatial branches when ω_i is large.

Figure 4 shows the evolution of the k-branches for $d = 0.01$, $X = 0.23$ as ω_i is decreased from a large positive value to $\omega_{0,i}$. This demonstrates that the two branches originate in opposite halves of the complex k-plane, thus satisfying the Briggs–Bers criterion. For the range of X-values used throughout the calculations this condition remained satisfied.

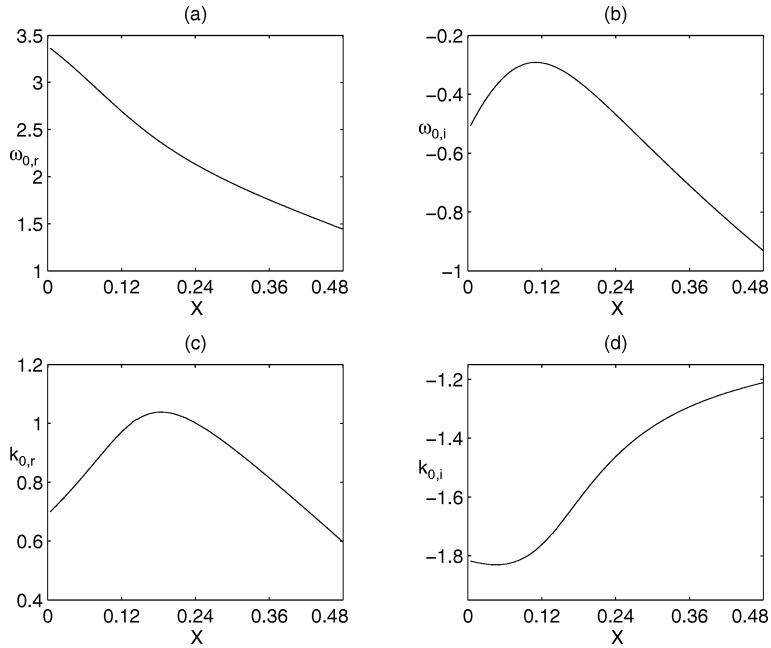

Figure 5. Absolute frequency (ω_0) and wavenumber (k_0) as a function of real X (up to $x^* = 4D^*$).

Figure 5 shows the absolute frequency ω_0 and wavenumber k_0 as a function of X. It can be seen that $\omega_{0,i} < 0$ for all X, so that the flow is absolutely stable and cannot therefore be globally unstable (Huerre and Monkewitz [7]), but there does exist a maximum in $\omega_{0,i}$ suggesting the existence of a saddle point X^t in the complex X-plane.

5.3. Location of the saddle point

The location of the saddle point can be identified by analytically continuing the data from the real X-axis into the complex X-plane using some appropriate approximating function. The usual choice would be to approximate by polynomials, but in this particular case severe problems occur because the saddle point is located high in the complex plane. This presents two problems—a low-order polynomial approximation behaves well when extended into the complex plane but is not sufficiently accurate in approximating the data on the real X-axis. On the other hand, a high-order polynomial captures the information on the real axis very accurately but is less well behaved high in the complex plane. As a result, approximation at different orders produces different values of X^t, making polynomial approximation unreliable. An alternative is to use rational function approximation, where the computed values of $\omega_0(X)$ are approximated by the form

$$R_n(X) = \frac{a_0 + a_1 X + a_2 X^2 + \cdots + a_n X^n}{1 + b_1 X + b_2 X^2 + \cdots + b_n X^n}. \tag{21}$$

This type of function tends to be better behaved when extended into the complex plane and produces convergence onto the desired location X^t as the order (n) of the approximation is increased.

The method used to obtain the best rational function fit involves a number of steps. A version of the Remes algorithm (see Ralston and Wilf [16] for details) is used to obtain a minimax solution, i.e. values of a_i and b_i

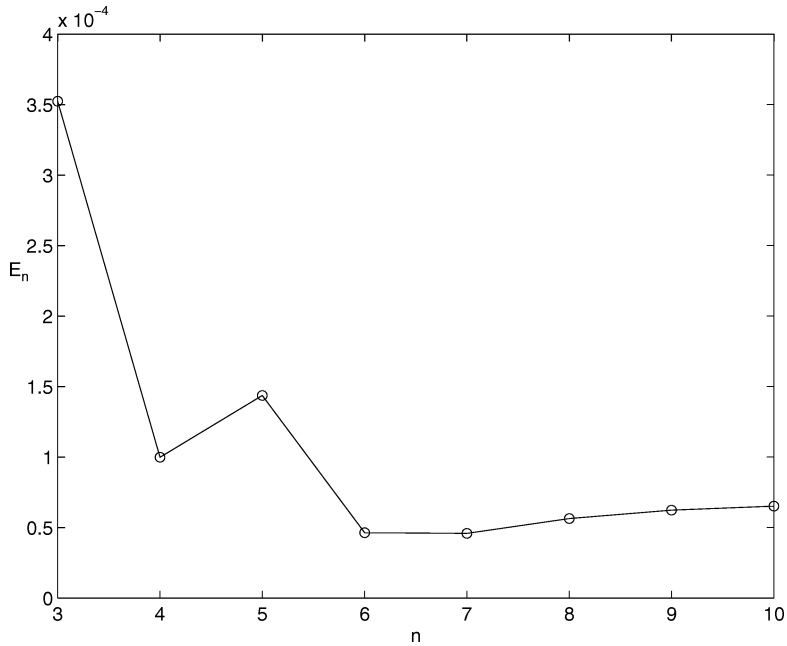

Figure 6. Error (E_n) in approximation of $\omega_0(X)$ with successive order (n) of rational function approximation.

which minimize the maximum deviation r_n, where

$$r_n = \max \left| R_n(X) - \omega_0(X) \right|.$$

For each value of n there exists a minimax solution and the value of n with the minimum value of r_n is selected as giving the best fit.

Figure 6 shows the error E_n between the minimax solution and the computed data, where the error is the root mean square

$$E_n = \sqrt{\frac{\sum_{j=1}^{N} |R_n(X_j) - \omega_0(X_j)|^2}{N}},$$

N being the number of data points along the X-axis. The minimum error occurs for $n = 7$ but there is little difference between this and the errors at $n = 6$ and higher orders. We proceed by considering the saddle point produced by the approximations at $n = 6$, 7 and 8 in order to monitor the accuracy of the analytic continuation technique.

Figure 7(*a*) shows zero contours of the real and imaginary parts of $\partial\omega_0/\partial X$ in the complex X-plane obtained from the rational function approximation. Points where the lines cross identify the value of X^t at which $\partial\omega_0/\partial X$ vanishes exactly. There is some slight variation in the location of X^t with the order of approximation, but this should be compared to the results in *figure 7*(*b*) which are obtained using polynomial approximation (i.e. $b_i = 0$ for $i = 1, \ldots, n$). Here the saddle-point location varies significantly as the order of the approximation is increased.

A comparison of the saddle-point location and the leading order global frequency is made in *table I* (with $d = 0.01$) for increasing values of n where the error in approximation (E_n) is comparable. This shows a clearly defined Strouhal number of the preferred mode, $S_D = 0.44$, which can be compared to experimental

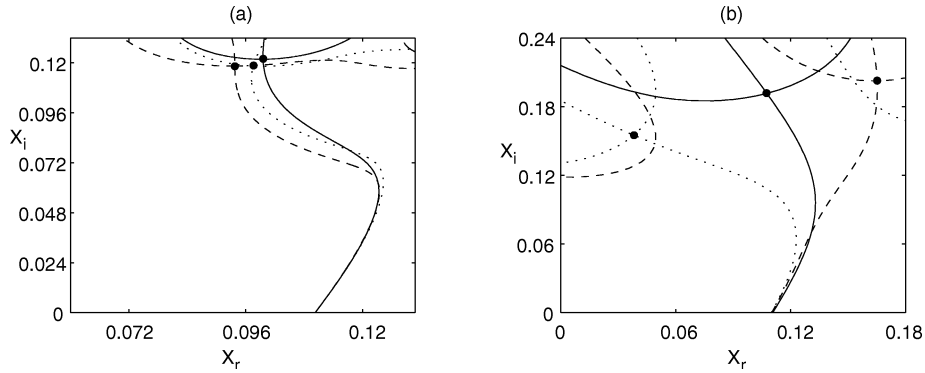

Figure 7. Contours of real and imaginary parts of $\partial\omega_0/\partial X = 0$ in complex X-plane. The point where two lines cross gives X^t for a given approximation. (a) Rational function approximation; (b) Polynomial approximation. Solid line: $n = 6$; dotted line: $n = 7$; dashed line: $n = 8$.

Table I. Comparison of saddle-point location and leading-order global frequency with increasing n (order of rational function approximation).

	Order of approximation for ω_0		
	$n = 6$	$n = 7$	$n = 8$
X^t	0.0996+0.1326i	0.0976+0.1186i	0.0938+0.1185i
ω_0^t	2.7563−0.7725i	2.7776−0.7666i	2.7926−0.7589i
St_D	0.4401	0.4421	0.4445

Table II. Numerical values at saddle-point given by $n = 7$ rational function approximation.

ω_{kk}^t	2.6949−0.3601i
ω_{0XX}^t	0.0914−0.7731i
k_0^t	0.7424−1.6485i
k_{0X}^t	−0.1783+0.2405i

values of 0.41 (Drubka [17]) and 0.45 (Kibens [18]) for the axisymmetric, low-subsonic near-top-hat jet. Experimental values for the preferred-mode Strouhal number have been found to range from $S_D = 0.3$ (Crow and Champagne [1]) up to about 0.5. The value of S_D observed in experiment or calculated theoretically is dependent to a considerable degree on the shape of the jet profile. A point to note here is that the values in *table I* have been computed for the ratio of length scales $d = 0.01$. Changes in the value of d however, only alter the position of the saddle point X^t, and do not change the value of ω_0^t or any of the associated parameters, so that the preferred-mode Strouhal number is independent of d.

Figure 8 shows the evolution of the ω_0-branch as X_i is increased for the $n = 7$ approximation. The cusp point in the ω_0-plane, for fixed X_i, is characteristic of the pinching of two branches in the complex X-plane, as sketched in *figure 2*. The value of ω_0 at the cusp point (ω_0^t) is the leading-order contribution to the global frequency.

The numerical procedure to determine $\omega_{kk}(X)$, for real X, involves the solution of an inhomogeneous Rayleigh equation (see Monkewitz et al. [4] for details). Subsequently both $k_0(X)$ and $\omega_{kk}(X)$ are analytically continued into the complex X-plane using a rational function approximation. The remaining parameters required for subsequent calculations are given in *table II*. In order to satisfy causality one must have $\omega_{kk,i} < 0$

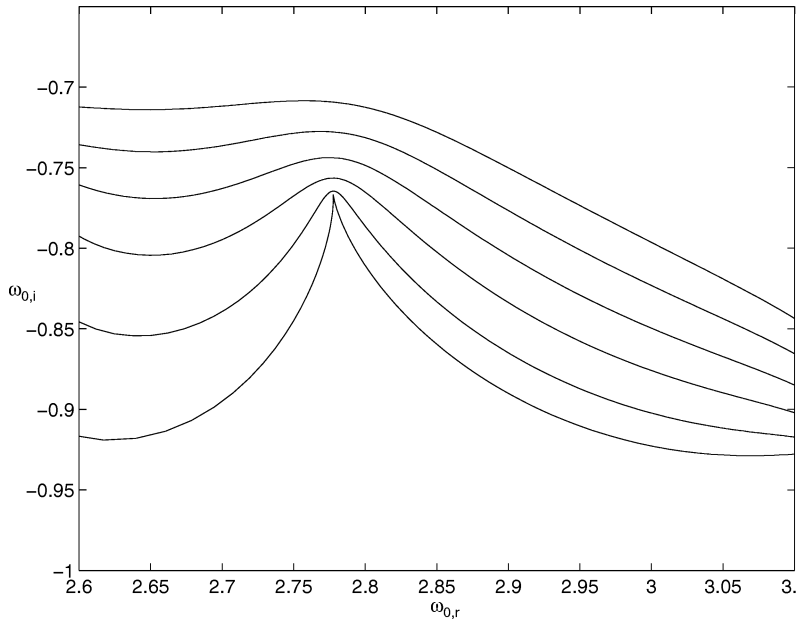

Figure 8. Evolution of ω_0 for constant values of X_i using the $n = 7$ rational function approximation. The uppermost line corresponds to $X_i = 0.09$; successive lines are for X_i increased in steps of 0.006 and the lower line is for $X_i = X_i^t$, where the characteristic cusp in the complex ω_0-plane identifies ω_0^t.

and $\omega_{0XX,i} < 0$ (Chomaz et al. [8]), and both of these conditions are found to be satisfied by the approximations used.

The axial variation of the global eigenfunction, using (9), can be written in terms of the unscaled streamwise coordinate x as follows,

$$A(x) = \exp\left[-\left\{\left(\frac{\omega_{0XX}^t}{\omega_{kk}^t}\right)^{1/2} - ik_{0X}^t\right\}\frac{\varepsilon}{2}\left(x - x^t\right)^2\right]\exp\left[ik_0^t\left(x - x^t\right)\right]. \tag{22}$$

The shape of the global mode amplitude can be calculated using the computed values appearing in *table II*.

5.4. Comparison with Laufer and Yen

In the experiments of Laufer and Yen [6] it was found that the amplitude of the near-field pressure fluctuations could be well modelled by a Gaussian function, with the width of that function being a fixed multiple of the instability wavelength at the frequency considered. They found their experimental data to collapse well onto the Gaussian form with $b/\lambda = 1.0$, where b is the Gaussian half-width and λ is the instability wavelength. The half-width b is defined as the $(x - x^t)$-value at which $|\bar{A}_0| = \exp(-1)$, and so from (22) that for the global mode is

$$b = \sqrt{\frac{2}{\varepsilon \mathrm{Re}\{(\omega_{0XX}^t/\omega_{kk}^t)^{1/2} - ik_{0X}^t\}}},$$

where Re{·} denotes the real part. The wavelength associated with the global mode is $2\pi/k^t_{0,r}$, and using values in *table II* the ratio is

$$b/\lambda = 0.2052/\sqrt{\varepsilon}. \tag{23}$$

Agreement with the Laufer and Yen [6] result occurs when $\varepsilon = 0.0421$, which corresponds to a shear-layer divergence rate of $\delta' = 0.0842$. Unfortunately, however, Laufer and Yen [6] did not present any mean profiles, so we have no direct way of checking this value of δ'. There is also no direct way of seeing how well the Laufer and Yen [6] profiles are represented by (16).

In terms of the acoustic field, the low Mach number experiments of Laufer and Yen [6] gave rise to acoustic fields which were superdirective in character, where the directivity varies exponentially with direction cosines, rather than in the low-order polynomial fashion expected from the general aeroacoustic theory of Lighthill [19]. The experimental results were found to follow the relation

$$\langle p^2 \rangle \sim \exp\{-45[1 - M_c \cos\theta]^2\}, \tag{24}$$

where M_c is the convection Mach number and θ is the angle from the jet exhaust. The θ-dependent part of (24), to leading order in M_c, is

$$\langle p^2 \rangle \sim \exp\{90 M_c \cos\theta\}. \tag{25}$$

Crighton and Huerre [5] obtained an expression for the acoustic field from a general Gaussian wavepacket. Using the Gaussian form in (22) determined by the global-mode theory, the sound field can be expressed as

$$p(r,\theta) \sim \frac{1}{\varepsilon^{1/2}} \left(\frac{2\pi M_c}{r}\right)^{1/2} \sin\theta \exp\left(i M_c r - \tfrac{1}{4} i\pi\right) \hat{A}\left(\frac{M_c \cos\theta - k^t_0}{(\varepsilon/2c)^{1/2}}\right), \tag{26}$$

where $c = 1/\{(\omega^t_{0XX}/\omega^t_{kk})^{1/2} - i k_{0X}\}$ and

$$\hat{A}(K) = \frac{1}{2\pi} \int_{-\infty}^{\infty} \exp\left(-\frac{\varepsilon x^2}{2c}\right) \exp(-iKx)\,\mathrm{d}x. \tag{27}$$

The θ-dependent part of the Gaussian, or 'antenna', factor of the expression in (26), to leading order in M_c, gives

$$\langle p^2 \rangle \sim \exp\left\{\frac{2}{\varepsilon}\left[c_r k^t_{0,r} - c_i k^t_{0,i}\right] M_c \cos\theta\right\}, \tag{28}$$

which is of the same form as that in (25).

Using computed values for c and k^t_0, and the value of $\varepsilon = 0.0421$, the result is

$$\langle p^2 \rangle \sim \exp\{76 M_c \cos\theta\}. \tag{29}$$

Thus the wavepacket for the lowest-order global mode yields a superdirective field, itself an astounding thing to find in a low Mach number acoustic field, even though it underestimates that found by Laufer and Yen. Experimental and theoretical results are compared, in *figure 9*, on a dB scale by plotting $10\log_{10}\langle p^2 \rangle$ over the range $0 \leqslant \theta \leqslant \pi/2$, using the results in (25) and (29), when $M_c = 0.075$. For a direct comparison, the value at $\theta = 0$ is taken to be 0 dB. Both curves show a significant variation from $\theta = 0$ to $\theta = \pi/2$, of ~ 29 dB from Laufer and Yen, and ~ 25 dB from the global-mode theory. The difference between these variations is, given all the imponderables of the calculation and the difficulties of the experiments at such low Mach number, remarkably small.

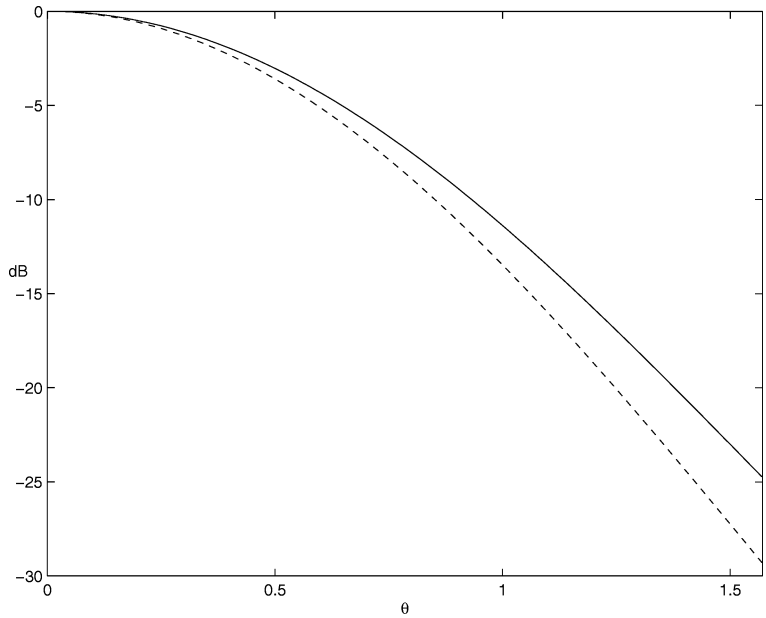

Figure 9. Variation of antenna factor with angle from jet exhaust (θ) on a dB scale; comparison between the global-mode theory result in (29) [solid line] and experimental results of Laufer and Yen [6] in (25) [dashed line].

6. Conclusions; and a conjecture

It has been shown that the slowly diverging, 'near-top-hat', axisymmetric jet sustains lightly damped global modes which can be excited to large amplitude (relative to background) by external forcing. Using analytic continuation into the complex X-plane—approximating numerical results with rational functions—leads to a well-defined global frequency. This predicts a preferred mode Strouhal number of $S_D = 0.44$, which lies within the range of experimentally predicted values (0.3–0.5). No criterion has previously been proposed which has led to the identification of any particular value.

The lowest-order global-mode amplitude has a Gaussian wavepacket structure and hence can give rise to a superdirective acoustic field, as suggested by the theory of Crighton and Huerre [5], and the experiments of Laufer and Yen [6]. Using numerical results from the global-mode calculation, both the near and far-fields have been compared to the results of Laufer and Yen [6]. A shear-layer divergence rate of $\delta' = 0.0842$ gives agreement with the Gaussian form of the near-field pressure fluctuations found by Laufer and Yen. The θ-dependent antenna factor in the directivity was determined by using the calculation of Crighton and Huerre [5] for the acoustic field. Substitution of numerical values associated with the lowest-order global mode gives rise to a pattern which agrees in part with that of Laufer and Yen. Although the form of the directivity is correct, the numerical values derived from it differ substantially from the Laufer and Yen levels. This is not altogether surprising, as unknown parameters appear in exponentials, there is no knowledge of the possible range of errors in the difficult Laufer and Yen experiments, and there is no information on their mean flow structure.

This investigation has been successful in describing—in terms of a global-mode structure—the case where there exists a preferred jet-column mode which is naturally lightly damped and is excited above background by external forcing, precisely as observed by Crow and Champagne [1]. The effects seen in the experiments of Laufer and Yen [6] can also be explained in part using the global-mode formulation. However in the experiments

of Bechert and Pfizenmaier [20] and Moore [21], it was found that broadband amplification occurred, in response to external single-frequency forcing, and no prominent tonal response. Crighton [22] studied results from a number of investigations in an attempt to link the two types of behaviour to some parameter differences. With Re_D the Reynolds number based on jet exit diameter and mean centre-line velocity, it was hypothesised that for $\mathrm{Re}_D < 10^5$ the jet response is of the preferred mode kind, but for $\mathrm{Re}_D > 10^5$ the response is the almost uniform broadband amplification and tonal suppression (see Table 1 of Crighton). These differences may be due to some change in the characteristics of the global mode. In particular, we conjecture that at a critical value of Re_D of order 10^5, the lowest-order global mode changes the sign of the imaginary part of its frequency, so that the mode becomes globally absolutely unstable. No linear model could be expected to predict the right behaviour for $\mathrm{Re}_D > 10^5$, and one would inevitably have to deal with a non-linear spatio-temporal system subject, in a typical experiment, to single-frequency external forcing. It is well known, at least in some model systems such as KdV and Sine-Gordon, that broadband chaotic response typically results from such single-frequency forcing.

In the model used here for the jet profile it is difficult to incorporate any effects of changing Reynolds number, and as such the model profile may be quite inadequate for investigation of the Reynolds number criterion conjectured above. The parameter $d = \delta_0^*/D^*$ is affected by changes in Reynolds number, but varying this parameter serves only to shift the location of the saddle point up or downstream, and has no effect on the global frequency value. A series of well-documented experimental jet profiles, taken across a range of Reynolds numbers, may provide insight into the different response seen apparently above $\mathrm{Re}_D \approx 10^5$. Ideally all these profiles would have thin and naturally turbulent shear layers at the nozzle exit, so that Reynolds number variations really would be the principal variations. A global-mode analysis using such profiles will be the subject of future work.

Acknowledgments

AJC acknowledges the support of a ROPA Research Grant awarded by the Mathematics Programme of the UK Engineering and Physical Sciences Research Council. We acknowledge with thanks helpful discussions with Dr. A. Iserles on the topic of analytic continuation.

It is a pleasure to be able to dedicate this article to Hans Fernholz in recognition of his service to the fluid dynamics community as a distinguished researcher, through his work for European Journal of Mechanics/B Fluids, and through his thirty five years of tireless work for EUROMECH and in thanks for innumerable personal kindnesses.

References

[1] Crow S.C., Champagne F.H., Orderly structure in jet turbulence, J. Fluid Mech. 48 (1971) 547–591.
[2] Michalke A., Instabilität eines kompressiblen runden Freistrahls unter Berücksichtigung des Einflusses der Strahlgrenzschichtdicke, Z. Flugwiss 19 (1971) 319–328.
[3] Crighton D.G., Gaster M., Stability of slowly diverging jet flow, J. Fluid Mech. 77 (1976) 397–413.
[4] Monkewitz P.A., Huerre P., Chomaz J-M., Global linear stability analysis of weakly non-parallel shear flows, J. Fluid Mech. 251 (1993) 1–20.
[5] Crighton D.G., Huerre P., Shear-layer pressure fluctuations and superdirective acoustic sources, J. Fluid Mech. 220 (1990) 355–368.
[6] Laufer J., Yen T.C., Noise generation by a low-Mach-number jet, J. Fluid Mech. 134 (1983) 1–31.
[7] Huerre P., Monkewitz P.A., Local and global instabilities in spatially developing flow, Ann. Rev. Fluid Mech. 22 (1990) 473–537.
[8] Chomaz J-M., Huerre P., Redekopp L.G., A frequency selection criterion in spatially developing flows, Stud. App. Math. 84 (1991) 119–144.
[9] Briggs R.J., Electron-Stream Interaction with Plasmas, MIT Press, 1964.
[10] Bers A., Linear waves and instabilities, in: DeWitt C., Peyraud J. (Eds), Physiques des Plasmas, Gordon & Breach, 1975, pp. 117–215.
[11] Bers A., Space-time evolution of plasma instabilities—absolute and convective, in: Rosenbluth M.N., Sagdeev R.Z. (Eds), Handbook of Plasma Physics, Vol. 1, North-Holland, 1983, pp. 451–517.

[12] Bender C.M., Orszag S.A., Advanced mathematical methods for scientists and engineers, McGraw-Hill, 1978.
[13] Pokrovskii V.L., Khalatnikov I.M., On the problem of above-barrier reflection of high energy particles, Soviet Phys. JETP 13 (1961) 1207–1210.
[14] Hille E., Ordinary Differential Equations in the Complex Domain, Wiley, 1976.
[15] Strange P.J.R., Crighton D.G., Spinning modes on axisymmetric jets. Part 1, J. Fluid Mech. 134 (1983) 231–245.
[16] Ralston A.,Wilf H.S., Mathematical Methods for Digital Computers, Wiley, New York, 1960.
[17] Drubka R.E., Instabilities in near field turbulent jets and their dependence on initial conditions and Reynolds number, PhD thesis, Inst. Technol., Chicago, 1981.
[18] Kibens V., The limit of initial shear layer influence on jet development, AIAA Paper 81-1960, 1981.
[19] Lighthill M.J., On sound generated aerodynamically I. General theory, Proc. Roy. Soc. Lond. A 221 (1952) 564–587.
[20] Bechert D., Pfizenmaier E., On the amplification of broadband jet noise by pure tone excitation, J. Sound Vib. 43 (1975) 581–587.
[21] Moore C.J., The role of shear-layer instability waves in jet exhaust noise, J. Fluid Mech. 80 (1977) 321–367.
[22] Crighton D.G., Acoustics as a branch of fluid mechanics, J. Fluid Mech. 106 (1981) 261–298.